Aalborg Universitet

HSS Modeling and Stability Analysis of Single-Phase PFC Converters

Gao, Guoqing; Wang, Xiongfei; Zhu, Tianhua; Liao, Yicheng; Tong, Jianli

Published in:
Conference Proceedings - IEEE Applied Power Electronics Conference and Exposition - APEC

DOI (link to publication from Publisher):
10.1109/APEC43599.2022.9773776

Publication date:
2022

Document Version
Accepted author manuscript, peer reviewed version

Link to publication from Aalborg University

Citation for published version (APA):
Gao, G., Wang, X., Zhu, T., Liao, Y., & Tong, J. (2022). HSS Modeling and Stability Analysis of Single-Phase PFC Converters. In *Conference Proceedings - IEEE Applied Power Electronics Conference and Exposition - APEC* (pp. 1812-1819). IEEE (Institute of Electrical and Electronics Engineers). https://doi.org/10.1109/APEC43599.2022.9773776

General rights
Copyright and moral rights for the publications made accessible in the public portal are retained by the authors and/or other copyright owners and it is a condition of accessing publications that users recognise and abide by the legal requirements associated with these rights.

- Users may download and print one copy of any publication from the public portal for the purpose of private study or research.
- You may not further distribute the material or use it for any profit-making activity or commercial gain
- You may freely distribute the URL identifying the publication in the public portal -

Take down policy
If you believe that this document breaches copyright please contact us at vbn@aub.aau.dk providing details, and we will remove access to the work immediately and investigate your claim.

Downloaded from vbn.aau.dk on: December 05, 2025

HSS Modeling and Stability Analysis of Single-Phase PFC Converters

Guoqing Gao[1], Xiongfei Wang[1], Tianhua Zhu[1], Yicheng Liao[2], Jianli Tong[3]
[1]AAU Energy, Aalborg University, Aalborg, Denmark
[2]School of Electrical Engineering and Computer Science, KTH Royal Institute of Technology, 100 44 Stockholm, Sweden
[3]Huawei technologies Co.Ltd, Xi'an, China
gga@energy.aau.dk, xwa@energy.aau.dk, tzh@energy.aau.dk, yichengl@kth.se, tongjianli@huawei.com

***Abstract*— The frequency coupling and low-frequency oscillations are common challenges faced by PFC converters in data centers. To reveal their mechanism, this paper proposes the systematic harmonic state space (HSS) modeling of the single-phase PFC converters and conducts the stability analysis on that basis. The HSS model is based on the linear time-periodic (LTP) theory, which can accurately reveal the frequency-coupling interactions. Besides, the developed HSS model is validated by the frequency scan. The stability analysis is performed and is shown to be consistent with the simulation results. In addition, a SISO equivalent impedance model of the single-phase PFC converters is proposed considering the frequency-coupling dynamics and the interaction with grid impedance, based on the MIMO impedance model derived from the HSS modeling.**

Keywords—PFC converter, harmonic state space, stability analysis, frequency coupling

I. Introduction

To conform with the standards on power factor and harmonics, the boost power factor correction (PFC) converters are extensively utilized in the AC-DC power conversion, especially in data centers as the principal power supplies [1, 2]. However, the low-frequency oscillations of PFC converters has been a plague of data center affecting the normal and efficient operation [3]. Hence, it is necessary to propose the accurate modeling methods and the suitable analysis tools to reveal the mechanism of frequency coupling and the low-frequency oscillation phenomena.

The boost PFC converter is essentially a time-periodic system. According to the different linearization methods, the modeling of PFC converters can mainly be divided into three categories:

1) Models based on double averaging
2) Models based on harmonic linearization
3) Models based on harmonic transfer function

The modeling of PFC converters based on double averaging can be further classified as two categories. To simplify this time-periodic system to a time-invariant model, the conventional double averaging [4] was proposed to derive the low-frequency averaged model of the output voltage by averaging the state variable over both a switching cycle and a rectifier line cycle. However, this method ignores all the harmonic dynamics of the state variables. Besides, the second type of double averaging was proposed in [5]. Similar with the double averaging method of [4], the averaging over a switching cycle was firstly applied. But in the second averaging step, the generalized averaging over the mains period was applied instead of using the moving average. This method was utilized for the period-doubling analysis, but it is not suitable for the frequency coupling dynamics analysis of the boost PFC converters.

The second category of modeling method is based on the describing function through harmonic linearization. The derived model based on describing function is the single-input and single-output (SISO) model, which fails to reveal the frequency-coupling dynamics [6]. The harmonic linearization was applied to the PFC converters in [7, 8] to obtain the input impedance for the impedance-based stability analysis. However, the describing function is based on the perturbation and response components of the same frequency. When the response is dominated by the sideband components of the perturbation frequency, the modeling based on the harmonic linearization will no longer be effective.

Considering that the boost PFC converter is a time-periodic system by nature, the LTP theory can be directly applied to linearize the system on periodic trajectories and the double averaging is no longer necessary. In addition, comparing with the models based on harmonic linearization, the harmonic state space (HSS) modeling [9, 10] based on the LTP theory is still valid even when the response is dominated by the sideband components of the perturbation frequency. Besides, the harmonic interactions of the boost PFC converters can be investigated through the derived harmonic transfer function. Therefore, the HSS modeling based on the LTP theory is applied in this paper and is validated by the frequency scan and the stability analysis.

In addition, the stability analysis of the boost PFC converters can mainly be classified as two categories:

1) The state-space based analysis (time domain)
2) The impedance-based analysis (frequency domain)

The modeling of boost PFC converter based on Floquet theory was proposed in [11] for the stability analysis and the identification of bifurcation types according to the eigenvalues of the transition matrix. The transition matrix [12] relates the values of the state variables from the beginning to the end of a period, which is conducive to the stability analysis of the LTP system. Besides, the LTP model of the single-phase active front end is derived in [13]. Then the significant eigenvalues of the harmonic state space model were utilized to determine the stability of the system. The stability analysis of the aforenoted two cases are all time-domain stability analysis methods based on the state-space models. However, this method has low modularity. The harmonic state space model needs to be rebuilt even with a minor change of the system structure. Therefore, the impedance-based stability analysis method is extended to

the MIMO model in this article, which can provide more physical insight of the interaction between the grid impedance and the boost PFC converter system and conduces to the design-oriented analysis. In addition, a simplified SISO impedance model of the boost PFC converters is proposed considering the frequency coupling dynamics and the interactions with grid impedance.

To reveal the mechanism of the frequency coupling phenomena and address the induced low-frequency oscillations, this paper first demonstrates the LTP characteristics and derives the harmonic transfer function of the boost PFC converters in part II. Then, the frequency coupling and stability analysis are conducted in part III and further validated by the frequency scan and FFT analysis. Finally, a SISO equivalent impedance model of the boost PFC converters is proposed in part IV.

II. HSS Modeling

A. Introduction of the Boost PFC Converter System

The schematic of the boost PFC converter system is illustrated in Fig. 1. The AC input v_g is connected to the boost converter through a diode rectifier. The controller mainly consists of the current control and the DC link voltage control. Typically, the bandwidth of the voltage loop is designed to be at least ten times lower than that of the current loop, which decouples the DC voltage and current loops [14]. Therefore, for the low-frequency oscillation phenomena, we have the following assumptions:

- Current control loop is ideal ($i_L(t)$ can be assumed to follow the reference $i_{ref}(t)$)
- Low frequency oscillation is caused by DC-link voltage control [8, 13]

According to the parametric scaling [15], when multiple identical boost PFC converters are connected in parallel, the equivalent simulation model can be obtained by scaling the grid inductance L_g, the inductance L of the boost converter, and the load resistance R by $1/N$. Besides, the capacitor C of the boost converter is scaled by N.

B. LTP Modeling of the Boost PFC Converter

The relationship between the input and output voltages of the boost PFC converter is shown as equation (1). The output voltage $v_{DC}(t)$ and the duty cycle $d(t)$ contain not only the DC

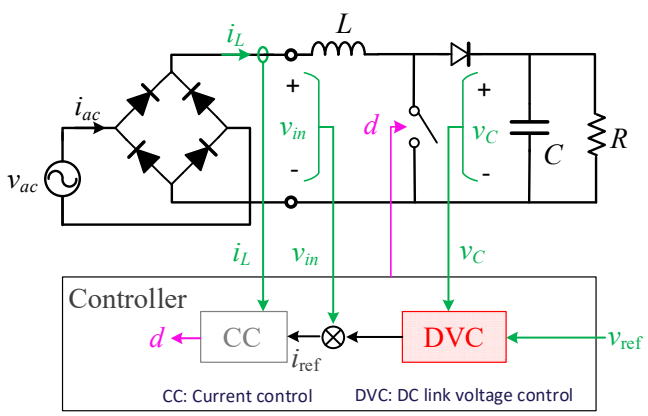

Fig. 1. The schematic of the boost PFC converter system

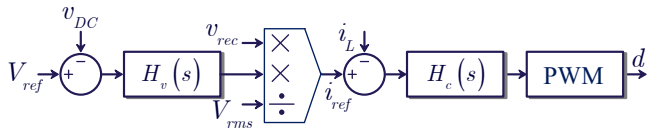

Fig. 2. The controller of the boost PFC converter

terms but also the time-periodic AC terms. Besides, the production of the state variables also introduces nonlinearity. Thus, the boost PFC converter is a nonlinear time-periodic system (NTP). This nonlinear time-periodic system can be linearized on the steady-state periodic trajectories to obtain a linear time periodic (LTP) model.

$$v_{rec}(t) = [1 - d(t)]v_{DC}(t) \tag{1}$$

The LTP models are used to describe the time-varying systems that exhibit the dynamics with periodic characteristics. The state space representation of the LTP system is expressed as

$$\begin{cases} \dot{x}(t) = \mathbf{A}(t)x(t) + \mathbf{B}(t)u(t) \\ y(t) = \mathbf{C}(t)x(t) + \mathbf{D}(t)u(t) \end{cases} \tag{2}$$

where $\mathbf{A}(t)$, $\mathbf{B}(t)$, $\mathbf{C}(t)$ and $\mathbf{D}(t)$ are periodic matrices varying in time t, with the fundamental frequency f_1.

For the boost PFC converter system, its topology and control structure are shown in Fig. 1 and Fig. 2, where $H_v(s)$ and $H_c(s)$ represent the voltage and current regulators, respectively. When the duty cycle d equals 1, the switch S is closed. Similarly, when the duty cycle d equals 0, the switch S is open. Therefore, the state-space averaging of the differential equations of the output voltage v_{DC} and the inductor current i_L within a switching cycle are shown in equation (3)

$$\begin{cases} C\dfrac{dv_{DC}}{dt} = (1-d)i_L - \dfrac{v_{DC}}{R} & \text{(a)} \\ L\dfrac{di_L}{dt} = v_{rec} - (1-d)v_{DC} & \text{(b)} \end{cases} \tag{3}$$

Considering that the dynamics of the current loop is much faster than that of the voltage loop, the current loop is assumed ideal when modeling the voltage loop. Therefore, the inductor current can be expressed as:

$$i_L(t) = i_{ref}(t) = \frac{u(t)v_{rec}(t)}{V_{rms}^2} \tag{4}$$

where $u(t)$ is the output of the voltage control loop and can be expressed as equation (5). k_p and k_i are proportional and integral coefficients, respectively. $v_{rec}(t)$ is the output voltage of the diode bridge, which is the rectified sine wave with the frequency of twice the main frequency.

$$u(t) = k_p\left(V_{ref} - v_{DC}(t)\right) + k_i\int_0^t\left(V_{ref} - v_{DC}(t)\right)\mathrm{d}t \tag{5}$$

After the state-space averaging of v_{DC} within a switching cycle as shown in equation (3), the model of the

boost PFC converter can be expressed as equation (6) via the simultaneous equations (1)(3)(4) and (5).

$$\begin{cases} \dfrac{\mathrm{d}v_{DC}(t)}{\mathrm{d}t} = -\dfrac{v_{DC}(t)}{CR} + \dfrac{v_{rec}^2(t)u(t)}{v_{DC}(t)V_{rms}^2 C} \\ \dfrac{\mathrm{d}u(t)}{\mathrm{d}t} = \dfrac{k_p v_{DC}(t)}{CR} - \dfrac{k_p v_{rec}^2(t)u(t)}{v_{DC}(t)V_{rms}^2 C} - k_i v_{DC}(t) + k_i V_{\mathrm{ref}} \end{cases} \tag{6}$$

The obtained model of (6) is a nonlinear time periodic system, which can be further linearized on the steady-state periodic trajectories $V_{\mathrm{DC}}(t)$, $U(t)$, $V_{\mathrm{rec}}(t)$ to get the small-signal linear time-periodic model as shown in equation (7).

$$\begin{cases} \dfrac{\mathrm{d}\tilde{v}_{DC}(t)}{\mathrm{d}t} = C_1(t)\tilde{v}_{DC}(t) + C_2(t)\tilde{u}(t) + C_3(t)\tilde{v}_{rec}(t) \\ \dfrac{\mathrm{d}\tilde{u}(t)}{\mathrm{d}t} = C_4(t)\tilde{v}_{DC}(t) + C_5(t)\tilde{u}(t) + C_6(t)\tilde{v}_{rec}(t) \end{cases}$$

$$C_1(t) = -\left(\frac{V_{rec}^2(t)U(t)}{V_{DC}^2(t)V_{rms}^2 C} + \frac{1}{RC}\right),\ C_2(t) = \frac{V_{rec}^2(t)}{V_{DC}(t)V_{rms}^2 C} \tag{7}$$

$$C_3(t) = 2\frac{V_{rec}(t)U(t)}{V_{DC}(t)V_{rms}^2 C},\ C_4(t) = \left(\frac{k_p V_{rec}^2(t)U(t)}{V_{DC}^2(t)V_{rms}^2 C} + \frac{k_p}{RC} - k_i\right)$$

$$C_5(t) = -\frac{k_p V_{rec}^2(t)}{V_{DC}(t)V_{rms}^2 C},\ C_6(t) = -2\frac{k_p V_{rec}(t)U(t)}{V_{DC}(t)V_{rms}^2 C}$$

C. Harmonic Transfer Function

The harmonic transfer function was firstly proposed by N. M. Wereley [8]. Accordingly, a SISO LTP system can be expressed as a MIMO LTI system, which is suitable to characterize the frequency coupling phenomena.

Taking the typical LTP system as shown in equation (2) for example, the time-periodic coefficients $\mathbf{A}(t)$, $\mathbf{B}(t)$, $\mathbf{C}(t)$, and $\mathbf{D}(t)$ can be expanded by Fourier series such as

$$\mathbf{A}(t) = \sum_{k=-\infty}^{+\infty} A_k e^{jkw_1 t} \tag{8}$$

Supposing that the time-periodic variables $x(t)$, $u(t)$, and $y(t)$ are exponentially modulated periodic (EMP) signals as shown in equation (9)

$$u(t) = e^{st}\sum_{k=-\infty}^{+\infty} U_k e^{jkw_1 t},\ x(t) = e^{st}\sum_{k=-\infty}^{+\infty} X_k e^{jkw_1 t},\ y(t) = e^{st}\sum_{k=-\infty}^{+\infty} Y_k e^{jkw_1 t} \tag{9}$$

Substituting equations (8) and (9) into (2) and applying the principle of harmonic balance, the LTP model in (2) can be expressed by the doubly infinite matrix equation as

$$\begin{aligned} s\mathcal{X} &= (\mathcal{A} - \mathcal{N})\mathcal{X} + \mathcal{B}\mathcal{U} \\ \mathcal{Y} &= \mathcal{C}\mathcal{X} + \mathcal{D}\mathcal{U} \end{aligned} \tag{10}$$

where $\mathcal{A}$ is the doubly infinite Toeplitz matrix formed by the Fourier coefficients of $\mathbf{A}(t)$ as shown in equation (11). Similarly, the Toeplitz matrices $\mathcal{B}$, $\mathcal{C}$ and $\mathcal{D}$ are obtained by utilizing the Fourier series coefficients of $\mathbf{B}(t)$, $\mathbf{C}(t)$ and $\mathbf{D}(t)$, respectively.

$$\mathcal{A} = \begin{bmatrix} \ddots & \vdots & \vdots & \vdots & \\ \cdots & A_0 & A_{-1} & A_{-2} & \cdots \\ \cdots & A_1 & A_0 & A_{-1} & \cdots \\ \cdots & A_2 & A_1 & A_0 & \cdots \\ & \vdots & \vdots & \vdots & \ddots \end{bmatrix} \tag{11}$$

Besides, $\mathcal{U}$, $\mathcal{Y}$ and $\mathcal{X}$ as shown in (12) represent the doubly infinite input, output, and the state vectors formed by the Fourier coefficients of $u(t)$, $y(t)$ and $x(t)$, respectively.

$$\mathcal{X} = \begin{bmatrix} \vdots \\ X_{-1}(s - jw_1) \\ X_0(s) \\ X_1(s + jw_1) \\ \vdots \end{bmatrix},\ \mathcal{U} = \begin{bmatrix} \vdots \\ U_{-1}(s - jw_1) \\ U_0(s) \\ U_1(s + jw_1) \\ \vdots \end{bmatrix},\ \mathcal{Y} = \begin{bmatrix} \vdots \\ Y_{-1}(s - jw_1) \\ Y_0(s) \\ Y_1(s + jw_1) \\ \vdots \end{bmatrix} \tag{12}$$

Finally, according to the harmonic state space model of (10), the harmonic transfer function is obtained as

$$\mathcal{Y} = \mathcal{H}(s)\mathcal{U} \tag{13}$$

where $\mathcal{H}(s) = \mathcal{C}\,[s\mathcal{I} - (\mathcal{A} - \mathcal{N})]^{-1}\,\mathcal{B} + \mathcal{D}$. The harmonic transfer function $\mathcal{H}$ expresses the relationship among the Fourier coefficients of the output and the input variables.

D. Harmonic State Space Modeling of the Boost PFC Converter

The HSS model can be derived based on the linear time-periodic model of the boost PFC converter system as illustrated in equation (7), where the state variables and coefficients are all time-periodic. They can be expressed in terms of their Fourier coefficients as the doubly infinite block Toeplitz matrices. Then the small-signal representation of the boost converters in Toeplitz matrix form is shown in equation (14)

$$\begin{cases} s\tilde{\mathcal{V}}_{DC}(s) = (\mathcal{C}_1 - \mathcal{N})\tilde{\mathcal{V}}_{DC}(s) + \mathcal{C}_2\tilde{\mathcal{V}}_{\mathrm{rec}}(s) + \mathcal{C}_3\tilde{\mathcal{U}}(s) \\ s\tilde{\mathcal{U}}(s) = \mathcal{C}_4\tilde{\mathcal{V}}_{DC}(s) + \mathcal{C}_5\tilde{\mathcal{V}}_{\mathrm{rec}}(s) + (\mathcal{C}_6 - \mathcal{N})\tilde{\mathcal{U}}(s) \\ \tilde{\mathcal{I}}_L(s) = \mathcal{C}_7\tilde{\mathcal{V}}_{\mathrm{rec}}(s) + \mathcal{C}_8\tilde{\mathcal{U}}(s) \end{cases} \tag{14}$$

Accordingly, the input admittance matrix of the boost converters is expressed as (15) with the simultaneous equations of (14).

$$\mathcal{Y}_{boost} = \frac{\tilde{\mathcal{I}}_L(s)}{\tilde{\mathcal{V}}_{\mathrm{rec}}(s)} \tag{15}$$

Besides, the illustration of the diode bridge in the boost PFC converter is shown in Fig. 3. The relationship of the

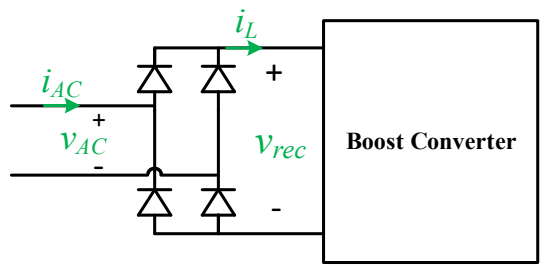

Fig. 3. The state variables of the diode bridge on the AC and DC sides

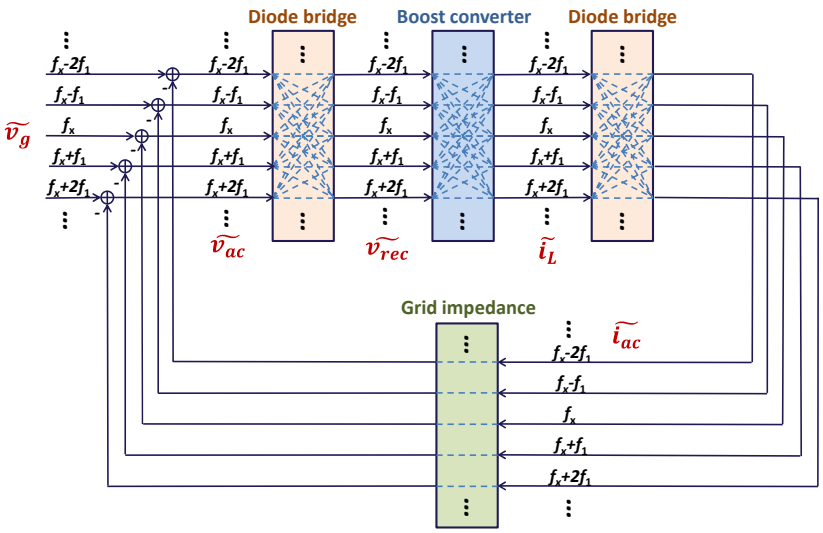

Fig. 4. Frequency-domain small-signal analysis of the Boost PFC converter system

state variables on the AC and DC sides of the diode bridge is expressed in (16), where $S_1(t)$ and $S_2(t)$ are switching functions of the diode bridge.

$$\begin{cases} v_{rec}(t) = S_1(t) v_{AC}(t) \\ i_{AC}(t) = S_2(t) i_L(t) \end{cases} \tag{16}$$

Applying the small-signal perturbations to all the variables in equation (16), then removing the steady state DC terms and discarding the second order AC terms (i.e. the product of the perturbations), the linearized small-signal model of the diode bridge is expressed as (17)

$$\begin{cases} \tilde{v}_{rec}(t) = S_{1s}(t) \tilde{v}_{AC}(t) + \tilde{S}_1(t) v_{ACs}(t) \\ \tilde{i}_{AC}(t) = S_{2s}(t) \tilde{i}_L(t) + \tilde{S}_2(t) i_{Ls}(t) \end{cases} \tag{17}$$

When a small-signal disturbance is applied to the input voltage v_{AC} of the diode bridge, a disturbance $\tilde{S}(t) = S_s(t) - S(t)$ in the switching function of the diode bridge will be generated. The disturbance of the switching function is a pulse signal with the magnitude of 2 in the vicinity of the voltage crossing points of v_{AC}, whereas with the magnitude of zero in other intervals. Considering that the input voltage v_{AC} and the output current i_L of the diode bridge is approximately zero in the voltage crossing points, the terms $\tilde{S}_1(t) v_{ACs}(t)$ and $\tilde{S}_2(t) i_{Ls}(t)$ in (17) are around zero and can be ignored. The remaining parts, e.g. the switching functions $S_{1s}(t)$ and $S_{2s}(t)$, are all time-periodic. They can be expressed in terms of their Fourier coefficients as the doubly infinite block Toeplitz matrices. Then the

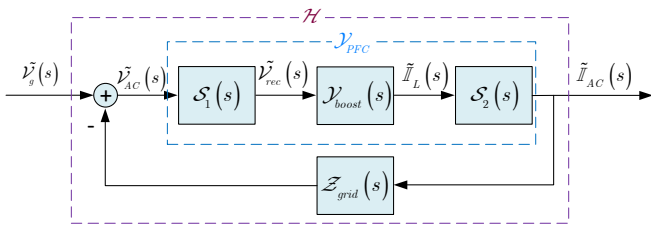

Fig. 5. Harmonic state space block diagram of the boost PFC converter system

input admittance matrix of the boost PFC converter in Toeplitz matrix form is shown as (18), where the input admittance $\mathcal{Y}_{boost}$ of the boost converter is expressed as (15).

$$\mathcal{H}_1 = \frac{\tilde{\mathbb{I}}_{AC}}{\tilde{\mathcal{V}}_{AC}} = \mathcal{S}_1 \mathcal{Y}_{boost} \mathcal{S}_2 \tag{18}$$

In order to investigate the frequency coupling phenomena in the boost PFC converter system, the frequency-domain small-signal analysis of the boost PFC converter system is shown in Fig.4. Due to the non-linearity introduced by the diode bridge and the boost converter, there are frequency-couplings among the state variables.

The relationship of the variables of the AC and DC sides of the diode bridge is shown in (17), where the switching function $S(t)$ of the diode bridge contains the odd multiples of the fundamental frequency f_1. Then the bilinear terms (the product between the state variables and the switching function) will lead to the frequency coupling phenomena. For example, assuming that there is a frequency perturbation at frequency f_x in the input voltage v_{ac}, the output voltage v_{rec} of the diode bridge will contain the different frequency components at $f_x \pm kf_1 \left(k = 1, 2, \ldots\right)$ besides the frequency components at f_x. In addition, the switching cycle averaged model of the boost converter is shown in (3). The bilinear terms will also introduce the frequency coupling between the input and output of the boost converter.

III. Stability Analysis

According to the derived input admittance matrix of the boost PFC converter as shown in (18) and considering the effect of grid impedance, the harmonic state space block diagram of the boost PFC converter system is illustrated in Fig. 5. Based on the block diagram of Fig. 5, the harmonic transfer function from the grid voltage v_g to the input current i_{AC} of the boost PFC converter is expressed as (19) in the Toeplitz matrix form.

$$\mathcal{H} = \frac{\tilde{\mathbb{I}}_{AC}}{\tilde{\mathcal{V}}_g} = \frac{\mathcal{Y}_{PFC}}{I + \mathcal{Y}_{PFC} \mathcal{Z}_{grid}} = \frac{\mathcal{S}_1 \mathcal{Y}_{boost} \mathcal{S}_2}{I + \mathcal{S}_1 \mathcal{Y}_{boost} \mathcal{S}_2 \mathcal{Z}_{grid}} \tag{19}$$

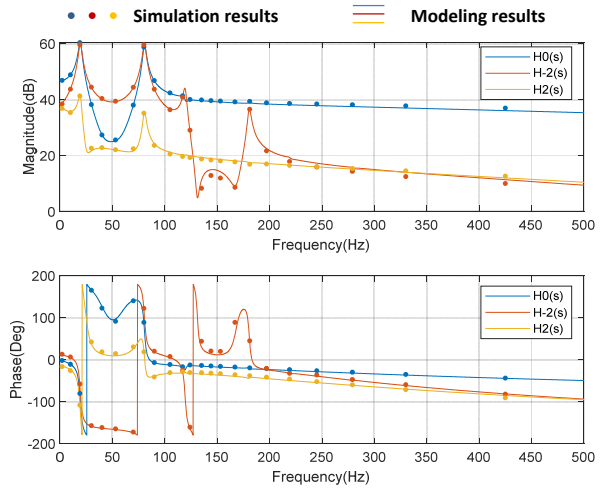

Fig. 6. Model validation with frequency scan

The detailed expression of the harmonic transfer function matrix $\mathcal{H}$ is shown as (20) in the bottom of this page. The harmonic order of the harmonic transfer function matrix $\mathcal{H}$ is selected when the elements of $\mathcal{H}$ (e.g. H_0, H_2) do not change significantly when the harmonics number is increased.

The harmonic transfer function can easily express the multiple frequency coupling phenomena in the boost PFC converter. For instance, a disturbance in v_g with the frequency of f_0 will lead to the disturbances in i_{AC} with different frequencies such as f_0, f_0+f_1, f_0-f_1, f_0+2f_1, f_0-2f_1. The elements of the transfer function matrix (e.g., $H_{-2}(s)$, $H_2(s)$ in equation (21)) represent the frequency coupling relationship between the perturbation frequency and the response frequency which is the sideband of the perturbation frequency.

$$H_0(s)=\frac{\tilde{I}_{AC}(s)}{\tilde{V}_g(s)},\ H_{-2}(s)=\frac{\tilde{I}_{AC}(s-2f_1)}{\tilde{V}_g(s)},\ H_2(s)=\frac{\tilde{I}_{AC}(s+2f_1)}{\tilde{V}_g(s)} \quad (21)$$

In order to validate the harmonic state space modeling of the multi-paralleled boost PFC converters system, the comparison between the modeling and simulation results is shown in Fig. 6. The HSS modeling results have a good match with the frequency scan. Besides, there is an interval around 50Hz, where $H_{-2}(s)$ is dominated instead of $H_0(s)$. Since $H_{-2}(s)$ represents the relationship between the perturbation at frequency f_x and the sideband component of the response at frequency f_1-f_x, it is not accurate to represent the input admittance of the boost PFC converter only with $H_0(s)$, which describes the relationship between the perturbation and the response both at frequency f_x without considering the sideband components.

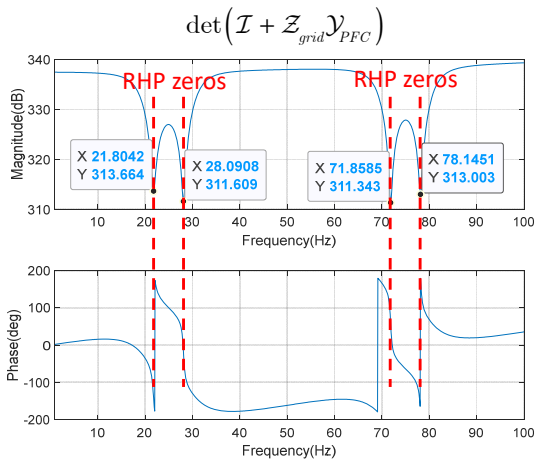

(a) L_g=0.132 p.u. (SCR=3.8)

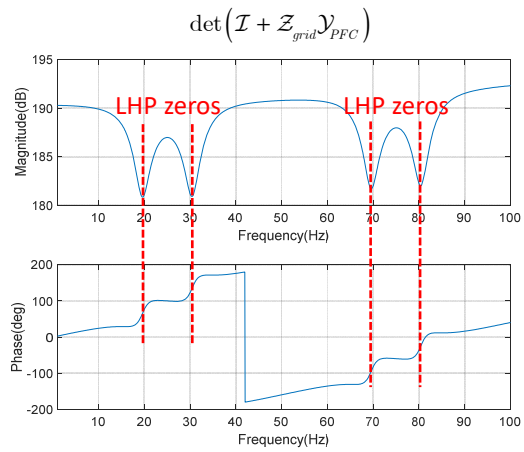

(b) Lg=0.076 p.u. (SCR=6.6)

Fig. 7. Bode plot of the characteristic equation.

Therefore, the multiple-input and multiple-output (MIMO) harmonic transfer function matrix as illustrated in Fig. 5 can be utilized to accurately investigate the frequency coupling phenomena and conduct the stability analysis.

The stability of the boost PFC converter system can be decided with the MIMO return ratio matrix $\mathcal{L}=\mathcal{Z}_{grid}\mathcal{Y}_{PFC}$. If all the zeros, z_1, z_2, … , z_{2n} of the characteristic equation as shown in equation (22) are located in the left-half plane, the PFC converter system will be stable [16, 17]. If there is a conjugate pair of right-half plane (RHP) zeros, the phase and magnitude plots will exhibit a step change of -180° and a slop change of +40dB/decade (with an anti-resonant peak if the damping ratio is less than 0.7), respectively. In contrary, a conjugate pair of RHP poles will lead to a step

$$\underbrace{\begin{bmatrix} \vdots \\ \tilde{I}_{AC}(f_0-2f_1) \\ \tilde{I}_{AC}(f_0-f_1) \\ \tilde{I}_{AC}(f_0) \\ \tilde{I}_{AC}(f_0+f_1) \\ \tilde{I}_{AC}(f_0+2f_1) \\ \vdots \end{bmatrix}}_{\tilde{\mathbb{I}}_{AC}} = \underbrace{\begin{bmatrix} \vdots & \vdots & \vdots & \vdots & \vdots & \vdots & \\ \cdots\ H_0(f_0-2f_1) & H_{-1}(f_0-f_1) & H_{-2}(f_0) & H_{-3}(f_0+f_1) & H_{-4}(f_0+2f_1) & \cdots \\ \cdots\ H_1(f_0-2f_1) & H_0(f_0-f_1) & H_{-1}(f_0) & H_{-2}(f_0+f_1) & H_{-3}(f_0+2f_1) & \cdots \\ \cdots\ H_2(f_0-2f_1) & H_1(f_0-f_1) & H_0(f_0) & H_{-1}(f_0+f_1) & H_{-2}(f_0+2f_1) & \cdots \\ \cdots\ H_3(f_0-2f_1) & H_2(f_0-f_1) & H_1(f_0) & H_0(f_0+f_1) & H_{-1}(f_0+2f_1) & \cdots \\ \cdots\ H_4(f_0-2f_1) & H_3(f_0-f_1) & H_2(f_0) & H_1(f_0+f_1) & H_0(f_0+2f_1) & \cdots \\ \vdots & \vdots & \vdots & \vdots & \vdots & \end{bmatrix}}_{\mathcal{H}} \underbrace{\begin{bmatrix} \vdots \\ \tilde{V}_g(f_0-2f_1) \\ \tilde{V}_g(f_0-f_1) \\ \tilde{V}_g(f_0) \\ \tilde{V}_g(f_0+f_1) \\ \tilde{V}_g(f_0+2f_1) \\ \vdots \end{bmatrix}}_{\tilde{\mathcal{V}}_g} \quad (20)$$

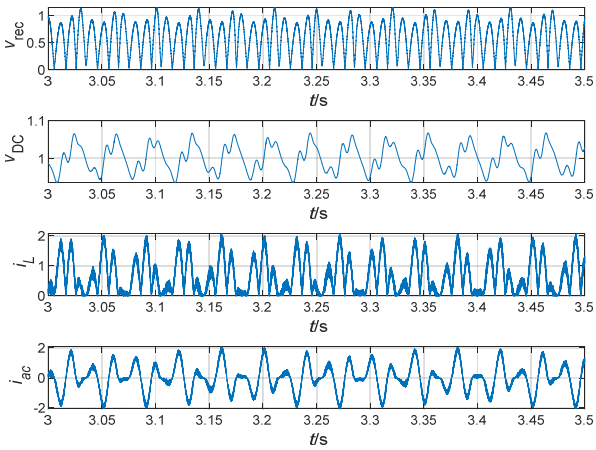

Fig. 8. The per unit time-domain waveforms of the state variables when L_g=0.132 p.u. (SCR=3.8)

change of 180° in the phase plot and a slop change of -40dB/decade (with a resonant peak if the damping ratio is less than 0.7) in magnitude plot, respectively. These criteria can be applied to the RHP poles or zeros identification of the characteristic equation.

$$\det\left(\mathcal{L}+\mathcal{I}\right)=0 \quad or \quad \det\left(\mathcal{Z}_{PFC}+\mathcal{Z}_{grid}\right)=0 \\ \Rightarrow z_1, z_2, \cdots, z_i \tag{22}$$

The Bode plots of the characteristic equation of the return ratio matrix with different grid impedance are shown in Fig. 7. There are anti-resonant peaks in the magnitude plot with the step change of -180° in the phase plot when the grid inductance L_g is about 0.132 p.u. (SCR=3.8), which indicates the RHP zeros of the characteristic equation. Therefore, the multi-paralleled boost PFC converters system is unstable in this case and is consistent with the time-domain simulation results as shown in Fig. 8. The fast Fourier transform (FFT) of the unstable time-domain waveforms of the state variables is illustrated in Fig.9. It is obvious that the frequencies of the main components of the FFT plot are consistent with the frequencies or coupling frequencies of the RHP zeros of Fig. 7. This phenomenon further validates the frequency coupling analysis of Fig. 4: a

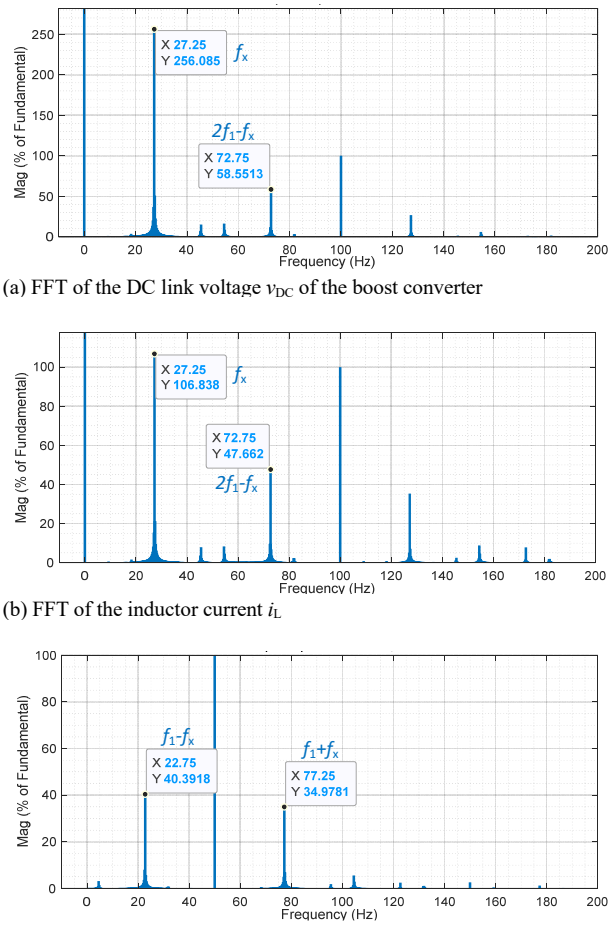

(a) FFT of the DC link voltage v_{DC} of the boost converter

(b) FFT of the inductor current i_L

(c) FFT of the input current i_{ac} of the boost PFC converter

Fig. 9. FFT of different state variables.

frequency component at f_x (the frequency of one of the RHP zeros) could introduce the different frequency components at $f_x \pm kf_1\left(k=1,2,\ldots\right)$.

IV. SISO Equivalent Impedance Model

Based on the MIMO impedance model of the boost PFC converter derived in part II, a SISO equivalent impedance

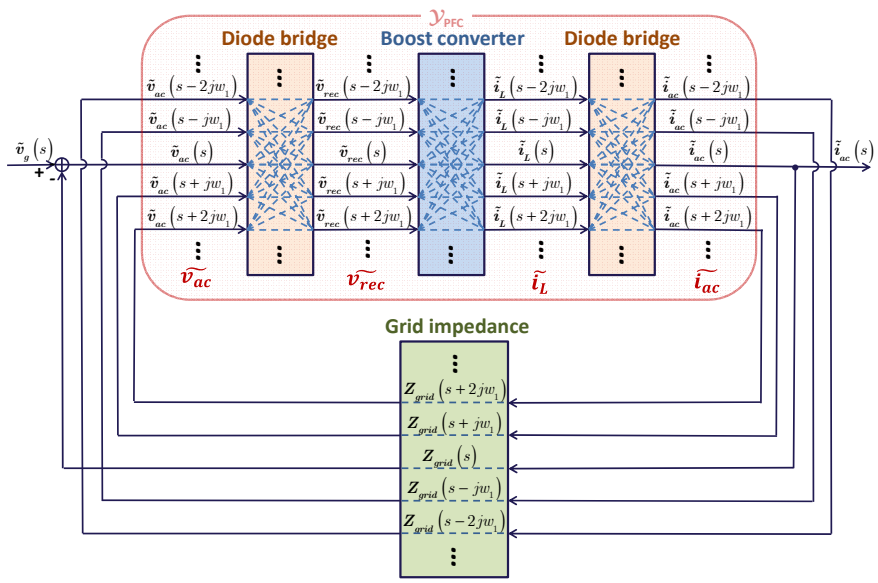

Fig. 10. Derivation of the equivalent SISO impedance model of the boost PFC converter system

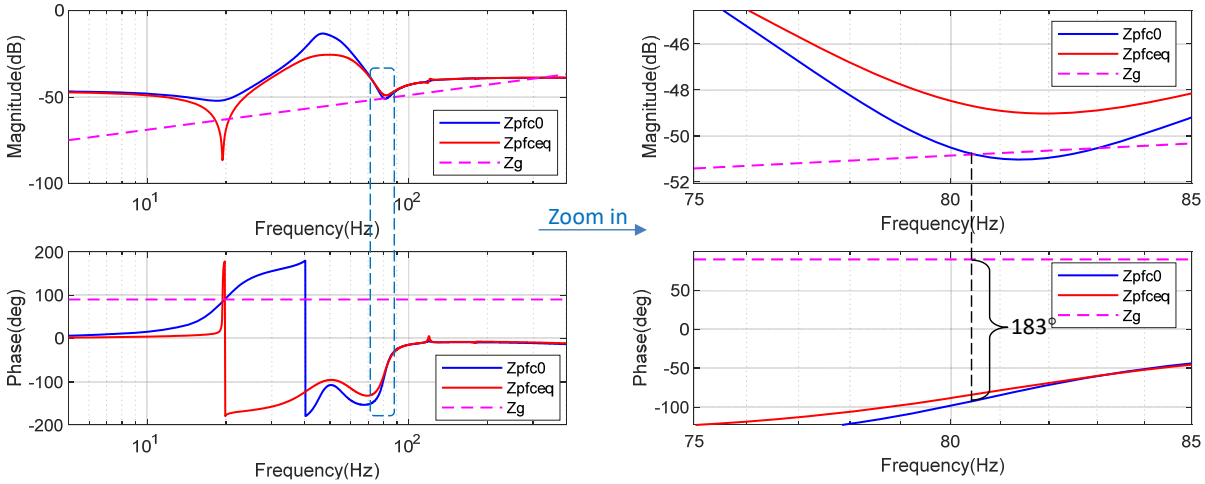

Fig. 12. The comparison of the bode plots of Zpfceq(s) and Zpfc0(s)

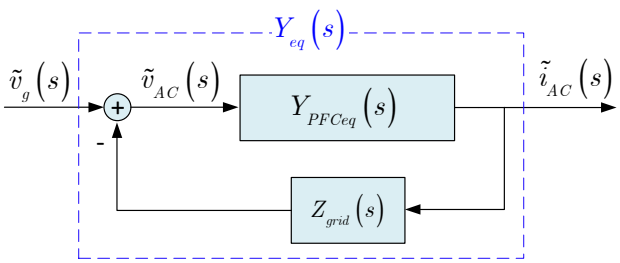

Fig. 11. Block diagram of the SISO equivalent impedance model of the boost PFC converters system

model of the grid-connected PFC converter is proposed in this part as illustrated in Fig. 10. Compared with the input impedance Z_{pfc0} of the boost PFC converter with the conventional SISO model [5, 7], the SISO equivalent model derived based on the MIMO impedance model of the PFC converter contains the frequency-coupling dynamics and the interaction with grid impedance.

The block diagram of the SISO equivalent impedance model of the multi-paralleled boost PFC converter system is shown in Fig. 11, where $Y_{eq}(s)$ represents the equivalent SISO impedance of the boost PFC converters interconnected with the grid. The expression of $Y_{eq}(s)$ is given by equation (23), which is actually the central elements of matrix $\mathcal{H}$ (N is the harmonic order of the HSS model) and therefore contains the frequency coupling dynamics of the PFC converters and their interactions with grid impedance.

$$Y_{eq}(s) = \frac{\tilde{i}_{AC}(s)}{\tilde{v}_{AC}(s)} = \mathcal{H}_{N,N}(s) \tag{23}$$

According to the equivalent SISO block diagram of Fig. 11 and the expression of $Y_{eq}(s)$, the equivalent SISO admittance $Y_{PFCeq}(s)$ of the boost PFC converters can be solved as expressed in equation (24). Although in the SISO form, the equivalent admittance $Y_{PFCeq}(s)$ contains the frequency-coupling dynamics of $\mathcal{Y}_{PFC}$ as illustrated in Fig. 10, as well as the interaction with grid impedance.

$$Y_{PFCeq}(s) = \frac{Y_{eq}(s)}{1 - Z_{grid}(s) Y_{eq}(s)} \tag{24}$$

In order to validate the accuracy of the equivalent SISO impedance model, the comparison of the bode plots between $Z_{pfceq}(s)$ and $Z_{pfc0}(s)$ is shown in Fig. 12, where $Z_{pfc0}(s)$ is the input impedance of the boost PFC converters without considering the frequency coupling and the interaction with grid impedance. When the grid inductor L_g is 0.08 p.u., the boost PFC converters system is stable according to the simulation results, whereas the phase difference between $Z_{pfc0}(s)$ and $Z_g(s)$ is greater than 180° at the magnitude intersection point, which indicates that the impedance model ignoring the frequency coupling dynamics is not accurate for the stability analysis.

V. Conclusions

This paper presents the detailed and systematic HSS modeling of single-phase PFC converters and introduces the stability analysis methods suitable for HSS models. An aggregated LTP model of the multi-paralleled boost PFC converters is derived and the MIMO HSS model is deduced on that basis. The frequency-coupling mechanism of the boost PFC converters is revealed with the MIMO impedance model. Besides, the proposed HSS model is validated through the frequency scan. The stability analysis is shown to be consistent with the simulation results and further explain the frequency coupling dynamics and the induced low-frequency oscillations. Finally, considering the frequency-coupling dynamics and the interaction with grid impedance, a SISO equivalent impedance model of the single-phase PFC converters is proposed based on the derived MIMO impedance model and is shown to be more accurate than the conventional SISO model ignoring the frequency coupling dynamics.

References

[1] J. Sun, S. Wang, J. Wang, and L. M. Tolbert, "Development of a Converter-Based Data Center Power Emulator," in *2021 IEEE Applied Power Electronics Conference and Exposition (APEC)*, 2021, pp. 126-133: IEEE.

[2] Z. Liao, N. C. Brooks, Z. Ye, and R. C. Pilawa-Podgurski, "A high power density power factor correction converter with a multilevel boost front-end and a series-stacked energy decoupling buffer," in *2018 IEEE Energy Conversion Congress and Exposition (ECCE)*, 2018, pp. 7229-7235: IEEE.

[3] M. A. Vitorino, L. F. S. Alves, R. Wang, and M. B. J. I. T. o. P. E. de Rossiter Corrêa, "Low-frequency power decoupling in single-phase applications: A comprehensive overview," vol. 32, no. 4, pp. 2892-2912, 2016.

[4] K. Mahabir, G. Verghese, J. Thottuvelil, and A. Heyman, "Linear averaged and sampled data models for large signal control of high power factor AC-DC converters," in *21st Annual IEEE Conference on Power Electronics Specialists*, 1990, pp. 372-381.

[5] W. Siu-Chung, C. K. Tse, M. Orabi, and T. Ninomiya, "The method of double averaging: an approach for modeling power-factor-correction switching converters," *IEEE Transactions on Circuits and Systems I: Regular Papers,* vol. 53, no. 2, pp. 454-462, 2006.

[6] X. Yue, X. Wang, and F. Blaabjerg, "Review of Small-Signal Modeling Methods Including Frequency-Coupling Dynamics of Power Converters," *IEEE Transactions on Power Electronics,* vol. 34, no. 4, pp. 3313-3328, 2019.

[7] M. Chen and J. Sun, "Low-Frequency Input Impedance Modeling of Boost Single-Phase PFC Converters," *IEEE Transactions on Power Electronics,* vol. 22, no. 4, pp. 1402-1409, 2007.

[8] J. Sun, M. Xu, M. Cespedes, and M. Kauffman, "Low-Frequency Input Impedance Modeling of Single-Phase PFC Converters for Data Center Power System Stability Studies," in *2019 IEEE Energy Conversion Congress and Exposition (ECCE)*, 2019, pp. 97-106.

[9] N. M. Wereley, "Analysis and control of linear periodically time varying systems," Massachusetts Institute of Technology, 1990.

[10] E. K. Hidir, I. Uyanik, and Ö. Morgül, "Harmonic transfer functions based controllers for linear time-periodic systems," *Transactions of the Institute of Measurement and Control,* vol. 41, no. 8, pp. 2171-2184, 2018.

[11] W. Faqiang, Z. Hao, and M. Xikui, "Analysis of Slow-Scale Instability in Boost PFC Converter Using the Method of Harmonic Balance and Floquet Theory," *IEEE Transactions on Circuits and Systems I: Regular Papers,* vol. 57, no. 2, pp. 405-414, 2010.

[12] S. C. Sinha, R. Pandiyan, and J. Bibb, "Liapunov-Floquet transformation: Computation and applications to periodic systems," 1996.

[13] V. Salis, A. Costabeber, S. M. Cox, A. Formentini, and P. Zanchetta, "Stability Assessment of High-Bandwidth DC Voltage Controllers in Single-Phase Active Front Ends: LTI Versus LTP Models," *IEEE Journal of Emerging and Selected Topics in Power Electronics,* vol. 6, no. 4, pp. 2147-2158, 2018.

[14] R. Z. Scapini, L. V. Bellinaso, and L. J. I. T. o. P. E. Michels, "Stability analysis of AC–DC full-bridge converters with reduced DC-link capacitance," *IEEE Transactions on Power Electronics,* vol. 33, no. 1, pp. 899-908, 2017.

[15] V. Purba, B. B. Johnson, M. Rodriguez, S. Jafarpour, F. Bullo, and S. V. Dhople, "Reduced-order Aggregate Model for Parallel-connected Single-phase Inverters," *IEEE Transactions on Energy Conversion,* vol. 34, no. 2, pp. 824-837, 2019.

[16] Y. Liao and X. Wang, "Impedance-Based Stability Analysis for Interconnected Converter Systems With Open-Loop RHP Poles," *IEEE Transactions on Power Electronics,* vol. 35, no. 4, pp. 4388-4397, 2020.

[17] X. Wang and F. Blaabjerg, "Harmonic Stability in Power Electronic-Based Power Systems: Concept, Modeling, and Analysis," *IEEE Transactions on Smart Grid,* vol. 10, no. 3, pp. 2858-2870, 2019.